

Elastic scattering of the proton drip-line nucleus ^8B off a $^{\text{nat}}\text{Pb}$ target at 170.3 MeV

Y. Y. Yang,^{1,2} J. S. Wang,^{1,*} Q. Wang,¹ D. Y. Pang,³ J. B. Ma,¹ M. R. Huang,¹ J. L. Han,¹ P. Ma,¹ S. L. Jin,^{1,2} Z. Bai,^{1,2} Q. Hu,^{1,2} L. Jin,^{1,2} J. B. Chen,^{1,2} N. Keeley,⁴ K. Rusek,^{4,5} R. Wada,¹ S. Mukherjee,⁶ Z. Y. Sun,¹ R. F. Chen,¹ X. Y. Zhang,¹ Z. G. Hu,¹ X. H. Yuan,¹ X. G. Cao,^{1,†} Z. G. Xu,¹ S. W. Xu,¹ C. Zhen,^{1,‡} Z. Q. Chen,¹ Z. Chen,^{1,2} S. Z. Chen,^{1,2} C. M. Du,^{1,2} L. M. Duan,¹ F. Fu,¹ B. X. Gou,^{1,2} J. Hu,¹ J. J. He,¹ X. G. Lei,¹ S. L. Li,¹ Y. Li,^{1,2} Q. Y. Lin,^{1,2} L. X. Liu,^{1,2} F. D. Shi,¹ S. W. Tang,^{1,2} G. Xu,^{1,2} X. Xu,^{1,2} L. Y. Zhang,^{1,2} X. H. Zhang,¹ W. Zhang,^{1,2} M. H. Zhao,^{1,2} Z. Y. Guo,¹ Y. H. Zhang,¹ H. S. Xu,¹ and G. Q. Xiao¹

¹*Institute of Modern Physics, Chinese Academy of Sciences, Lanzhou, 730000, China*

²*University of Chinese Academy of Sciences, Beijing, 100049, China*

³*School of Physics and Nuclear Energy Engineering, Beihang University, Beijing 100191, China*

⁴*National Centre for Nuclear Research, ul. Andrzeja Sołtana 7, 05-400 Otwock, Poland*

⁵*Heavy Ion Laboratory, University of Warsaw, ul. Pasteura 5A, PL-02-093 Warsaw, Poland*

⁶*Physics Department, Faculty of Science, M.S. University of Baroda, Vadodara - 390002, India*

(Received 23 January 2013; published 29 April 2013; corrected 27 June 2013)

The elastic scattering of ^8B by a $^{\text{nat}}\text{Pb}$ target was measured at an incident energy of 170.3 MeV. Special care was taken with the limited intensity and broad profile of the secondary beam. The measured angular distribution of the differential cross section shows that the Coulomb-nuclear interference peak (CNIP) is not suppressed in this system, in contrast to what was observed in the scattering of neutron halo nuclei by heavy targets at energies around the Coulomb barrier. Analyses of the angular distribution were performed both in terms of the optical model using a single-folding-type potential and the continuum discretized coupled-channels (CDCC) method, which explicitly takes into account the breakup-channel couplings to the elastic scattering. The overall pattern of the differential cross section is well reproduced by the CDCC calculations. The calculations show that the effect of breakup-channel couplings on the elastic scattering is small in the present case.

DOI: [10.1103/PhysRevC.87.044613](https://doi.org/10.1103/PhysRevC.87.044613)

PACS number(s): 25.60.Bx, 25.70.Bc

I. INTRODUCTION

Reactions induced by light nuclei far from the β -stability valley, such as ^6He , ^{11}Be , ^8B , and others, are very interesting subjects. Many experimental and theoretical efforts have been devoted to the study of halo nuclei in order to investigate their unusual features [1–3]. However, they have not yet been fully explored. The striking feature of halo nuclei is the long tail of their matter density due to their weak binding energy. It has been found that the elastic scattering, a simple process, is a useful probe to study the size and surface diffuseness of exotic nuclei by comparing similarities and differences in reactions induced by weakly bound and tightly bound nuclei. Many interesting phenomena have been discovered by studying the elastic-scattering angular distributions for light neutron-halo nuclei near the Coulomb barrier. A great deal of elastic-scattering experiments have been performed for neutron-halo nuclei, such as ^6He [4–11] and ^{11}Be [12,13]. However, elastic-scattering data for proton-halo nuclei above the Coulomb barrier are still scarce.

It is well known that ^8B , with a proton separation energy of 0.1375 MeV, is a typical example of a pronounced proton-halo nucleus. Moreover, ^8B plays a prominent role in the solar neutrino problem. Thus, the structure and reaction mechanism

of ^8B have received much attention from both theoretical and experimental points of view. Many experiments with ^8B as a projectile have been performed. The total cross sections, fusion cross sections, breakup cross sections, electric quadrupole moment, and longitudinal momentum distributions of ^7Be fragments produced in (^8B , $^7\text{Be} + p$) breakup reactions have been measured [14–24]. Some elastic-scattering experiments have also been reported for ^8B on the light-mass target ^{12}C [25–27] and the intermediate-mass target ^{58}Ni [28].

Recently, $^{11}\text{Be} + ^{64}\text{Zn}$ elastic scattering near the Coulomb barrier exhibited the almost complete suppression of the Coulomb-nuclear interference peak (CNIP) [13]. It was suggested that this phenomenon was caused by both nuclear and Coulomb breakup couplings [29]. Similar features were observed earlier in the elastic scattering of neutron halo nuclei such as ^6He [7,8] by heavy targets, where they were found to be due largely to Coulomb breakup couplings alone. It is interesting to see whether this phenomenon exists for proton halo nuclei.

In the present paper, we report new experimental data for the elastic scattering of ^8B on a heavy target, $^{\text{nat}}\text{Pb}$, at 170.3 MeV. These data show no CNIP reduction in the elastic-scattering angular distribution for the proton-halo projectile ^8B at an energy around three times the Coulomb barrier. A brief description of the experimental setup and an outline of the data analysis are given in Sec. II. In Sec. III the measured elastic-scattering angular distributions are compared with optical model and continuum discretized coupled-channels (CDCC) calculations and the results are discussed. In Sec. IV the main conclusions of this work are summarized.

*jswang@impcas.ac.cn

[†]Present address: Shanghai Institute of Applied Physics, Chinese Academy of Sciences, Shanghai, 201800, China.

[‡]Present address: Institute of Modern Physics, Fudan University, Shanghai, 200433, China.

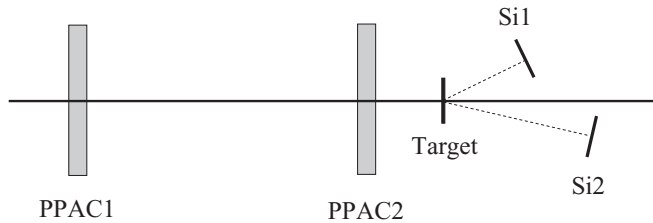


FIG. 1. Schematic view of experimental setup.

II. EXPERIMENTAL SETUP AND DATA ANALYSIS

A detailed description of the experimental setup and data analysis procedure used in this work can be found in Ref. [30] and therefore only brief descriptions are presented here. The angular distribution for the elastic scattering of ^8B by a natural Pb target was measured at $E_{\text{lab}} = 170.3$ MeV. The ^8B secondary beam, with contaminants of ^7Be , ^9C , and ^6Li ions, was produced by the Radioactive Ion Beam Line in Lanzhou (RIBLL) [31,32]. The secondary beam was produced by the fragmentation of a 54.2 MeV/nucleon ^{12}C primary beam, delivered by the Heavy Ion Research Facility of Lanzhou (HIRFL) [33,34], on a 2615 μm Be target. Although the magnetic field of the dipoles and quadrupoles of RIBLL was adjusted to focus on the ^8B secondary beam, contaminants with the same magnetic rigidity such as ^7Be , ^9C , and ^6Li were also present. Secondary beam particle identification was made using a combination of the measured time of flight (TOF) and the magnetic rigidity ($B\rho$) value. The average primary beam intensity during the measurements was about 300 eA with a ^{12}C charge state, producing ^8B and ^7Be beams of 5×10^2 and 5×10^3 particles per second, respectively. The experimental setup is shown in Fig. 1. Two position-sensitive parallel-plate avalanche counters (PPACs), developed at the Institute of Modern Physics, Chinese Academy of Sciences, provided the position and timing of the incoming beams with a position resolution of 1 mm. Each PPAC has 80 gold-plated tungsten wires in both X and Y directions and a sensitive area of 80×80 mm 2 . The tungsten wires, 50 μm in diameter, were spaced 1 mm apart. The signals from the strip electrodes were connected to a delay line with 4 ns delay between neighboring wires. The position information was then given by the time difference between the signals from both ends. The distances of PPAC1 and PPAC2 from the target were 500 mm and 100 mm, respectively. The position and incident angle of the beam particles at the target were determined by extrapolating the position information provided by PPAC1 and PPAC2 event by event.

The $^{\text{nat}}\text{Pb}$ target is a self supporting foil with a thickness of 4.2 mg/cm 2 . Two ΔE - E silicon-detector telescopes (denoted by Si2 and Si1 in Fig. 1), covering the polar angles 4° – 21° and 13° – 38° in the laboratory frame, respectively, were used to measure the energy and angle of elastically scattered particles. A large angular overlap was made in order to crosscheck the differential cross sections measured by the two telescopes. Each telescope consisted of one ΔE double-sided silicon strip detector (DSSD) with a thickness of 150 μm and an area of 48×48 mm 2 , and one single silicon detector (SSD) with a thickness of 1500 μm and an area of 50×50 mm 2 . The

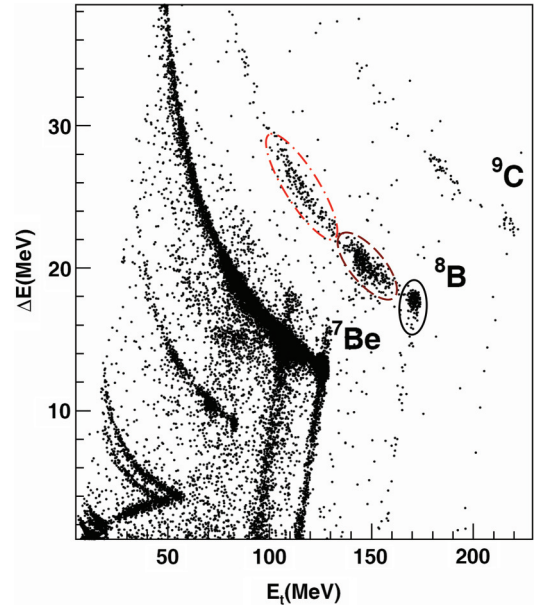


FIG. 2. (Color online) Typical ΔE - E_t particle identification spectrum of one strip from the Si2 telescope. The solid line ellipsoid encloses events corresponding to the elastic scattering from the $^{\text{nat}}\text{Pb}$ target, the dashed and dot-dashed ellipsoids enclose events corresponding to a single hit and two sequential hits of tungsten wires in the PPACs, respectively.

distances from the target center to the center of the DSSDs were 250 and 120 mm, respectively. The strip width of the DSSDs was 1 mm on both sides.

A typical ΔE - E_t particle identification spectrum obtained in the Si2 telescope is shown in Fig. 2. ΔE is the energy loss in the ΔE detector, and E_t is the sum of the energies deposited in both detectors of the telescope. One should note that good separation was obtained between the ^8B and the contaminants as well as between the elastically scattered and other reaction events. Three different regions on the ^8B line are identified: ^8B resulting from the elastic scattering on the $^{\text{nat}}\text{Pb}$ (solid line ellipsoid), ^8B scattered from a single hit on a tungsten wire of the PPACs (dashed ellipsoid) and ^8B scattered from double-sequential hits on the tungsten wires (dot-dashed ellipsoid).

The ^8B scattering angle can be obtained from the position information given by the two PPACs in the beam line and the telescopes. Since the secondary beam spot is large and nonuniform, the profile of the ^8B beam on the target cannot be viewed as a point compared with the distance between the target and the detectors. In order to overcome this disadvantage, a Monte Carlo simulation was made to evaluate the absolute differential cross section. The angular distribution of the elastic-scattering differential cross section was obtained as

$$\frac{d\sigma(\theta)}{d\sigma_{\text{Ruth}}(\theta)} = C \frac{N(\theta)_{\text{expt}}}{N(\theta)_{\text{Ruth}}}, \quad (1)$$

where C is a normalization constant, $N(\theta)_{\text{expt}}$ is the yield of ^8B elastic events at laboratory angle θ , and $N(\theta)_{\text{Ruth}}$ is the Rutherford scattering yield from the simulation. The normalization constant is a global normalization factor,

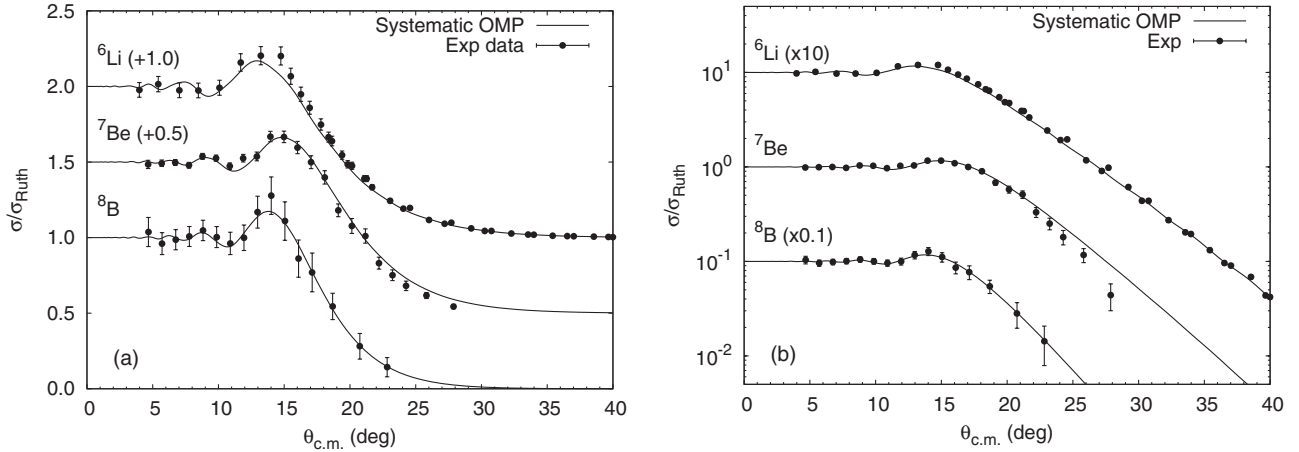


FIG. 3. Comparison between optical model calculations with the systematic single-folding potentials and experimental data for 99 MeV ${}^6\text{Li} + {}^{208}\text{Pb}$ elastic scattering [40], 125 MeV ${}^7\text{Be} + {}^{\text{nat}}\text{Pb}$ quasielastic scattering [30] and 170.3 MeV ${}^8\text{B} + {}^{\text{nat}}\text{Pb}$ quasielastic scattering. The Y axes are plotted on (a) linear and (b) logarithmic scales.

determined by supposing that the elastic scattering cross section is pure Rutherford scattering at small scattering angles. In order to minimize systematic errors, small corrections for detector misalignment were also performed using the method described in Ref. [30]. The ratio between the measured elastic differential cross section and the Rutherford cross section, $d\sigma/d\sigma_{\text{Ruth}}$, as a function of the center-of-mass angle $\theta_{\text{c.m.}}$, is shown in Fig. 3. In fact, these data are actually quasielastic scattering since some inelastic-scattering channels were not resolved due to the experimental energy resolution. However, as demonstrated in the following section, they may be regarded as pure elastic scattering for all practical purposes.

III. THEORETICAL ANALYSIS

In this section we present the results of optical model and CDCC calculations and their comparison with the experimental data. Coupled-channel calculations including low-lying collective states of the target were also performed to examine the inelastic contribution to the measured differential cross sections. For simplicity, these calculations assumed a pure ${}^{208}\text{Pb}$ target, although the experiment was performed with a natural lead target.

Recently, Xu and Pang derived a systematic nucleus-nucleus potential which can reasonably account for the elastic scattering and total reaction cross sections for projectiles with $A > 6$, including both stable and unstable nuclei, on heavy targets with $A \gtrsim 40$ for incident energies from near the Coulomb barrier to around 100 MeV/nucleon [35]. This potential is based on a single-folding model [36,37] using the Bruyères Jeukenne-Lejeune-Mahaux (JLMB) semimicroscopic systematic nucleon-nucleus potential [38,39]. Optical model calculations employing this systematic single-folding potential are compared with the experimental ${}^6\text{Li} + {}^{208}\text{Pb}$ [40] elastic scattering and ${}^7\text{Be}$ [30] and ${}^8\text{B} + {}^{\text{nat}}\text{Pb}$ quasielastic-scattering angular distributions at 99, 125, and 170.3 MeV, respectively, as shown in Fig. 3. All these energies are around three times the respective Coulomb barriers. Nucleon density

distributions for the projectile and target nuclei are needed in the single-folding calculations. The proton and neutron density distributions for ${}^6\text{Li}$ were obtained from independent-particle model calculations [41,42], in which the root-mean-square (rms) radius of ${}^6\text{Li}$ is obtained as 2.401 fm, close to the experimental value of 2.43 ± 0.02 fm [43]. The ${}^7\text{Be}$, ${}^8\text{B}$, and ${}^{208}\text{Pb}$ densities were obtained from Hartree-Fock calculations with the SKX interaction [44]. The rms radii of the proton distributions were 2.371 fm (2.36 ± 0.02 fm [14]), 2.537 fm (2.49 ± 0.03 fm [16]), and 5.441 fm (5.442 ± 0.02 fm [45]) for ${}^7\text{Be}$, ${}^8\text{B}$, and ${}^{208}\text{Pb}$, respectively. The numbers in parentheses are the corresponding experimental values. The total reaction cross sections obtained with the systematic single-folding model potentials were 3089 mb, 3062 mb, and 3270 mb for ${}^6\text{Li}$, ${}^7\text{Be}$, and ${}^8\text{B}$, respectively.

The agreement between the optical model calculations and the experimental data is good, suggesting that the contribution from inelastic-scattering channels to the ${}^7\text{Be}$ and ${}^8\text{B}$ quasielastic scattering is negligible. This will be explicitly demonstrated with the aid of coupled-channel calculations for ${}^8\text{B} + {}^{\text{nat}}\text{Pb}$; the case of interest here.

Since the first-excited state of ${}^8\text{B}$ is particle unstable, the scattered ${}^8\text{B}$ nuclei are necessarily all in the ground state. Thus we need only consider the contribution to the measured quasielastic-scattering cross section from inelastic excitations of the target nucleus. In order to estimate the effect of these inelastic contributions, coupled-channel calculations were performed with the code FRESKO [46] including excitation of the first 3^- (2.614 MeV) and the first 2^+ (4.086 MeV) states of ${}^{208}\text{Pb}$. Both Coulomb and nuclear excitations were included with reduced matrix elements $\langle 3^- || M(E3) || 0^+ \rangle = 815 e \text{ fm}^3$ and $\langle 2^+ || M(E2) || 0^+ \rangle = 55 e \text{ fm}^2$ and deformation lengths of $\delta_3 = 0.56$ fm and $\delta_2 = 0.43$ fm. These parameters were found to account well for the inelastic-scattering cross sections in the ${}^{28}\text{Si} + {}^{208}\text{Pb}$ system at 209.8 MeV [47]. The results of the coupled-channel calculations are shown in Fig. 4. It is observed that, even at the largest measured angle; namely, at around 23° in the c.m. system, the inelastic cross sections are about two orders of magnitude smaller than the elastic cross

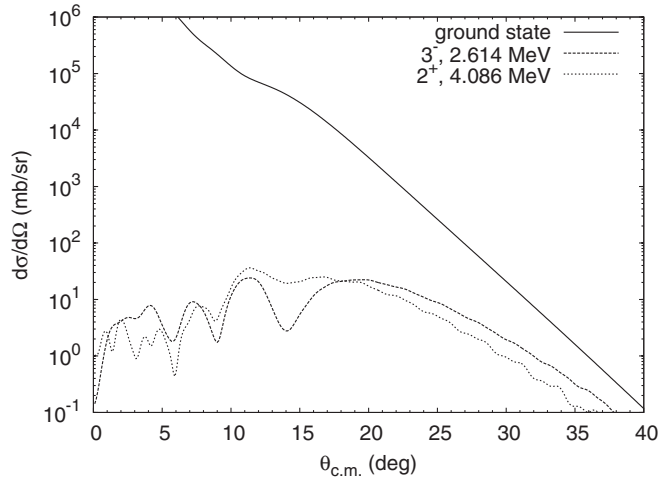


FIG. 4. Angular distributions of differential cross sections for elastic scattering and inelastic scattering to the first 3^- and 2^+ states of ^{208}Pb , shown as solid, dashed, and dotted curves, respectively.

section. These results confirm that, as suggested by the good agreement of the single-channel optical model calculation, the inelastic contribution to the quasielastic-scattering data is negligible.

CDCC calculations were performed using the code FRESKO [46] to investigate the influence of couplings to projectile breakup channels on the elastic scattering. The calculations used a standard three-body model in which the ^8B was modeled as a valence proton plus an inert ^7Be core. The spins of both the proton and the ^7Be were omitted. Test calculations confirmed that omitting the spins makes a negligible difference to both the elastic-scattering angular distribution and the total breakup cross section. The p - ^7Be binding potential was of Woods-Saxon form with parameters $r_0 = 1.149$ fm ($R = 2.198$ fm) and $a_0 = 0.602$ fm, taken from Ref. [48] (the spin-orbit component being omitted due to the absence of proton spin in our model). The depth was adjusted to give the correct proton binding energy for the ground state of ^8B (0.1375 MeV) and was fixed for the calculation of the continuum states. Proton- ^7Be relative orbital angular momenta up to $\ell = 3$ were included with all couplings up to multipolarity $\lambda = 3$. The continuum was discretized up to a maximum p - ^7Be relative energy of $\varepsilon_{\text{max}} = 15.3$ MeV, corresponding to $k_{\text{max}} = 0.8$ fm $^{-1}$, divided into eight equally spaced bins of width 0.1 fm $^{-1}$, giving a total of 32 bins. Convergence of elastic-scattering and breakup cross sections was verified by calculations with an increased model space with $k_{\text{max}} = 1.0$ fm $^{-1}$ and $\ell = 4$, $\lambda = 4$. The systematic single-folding potential described above was used for the $^7\text{Be} + ^{208}\text{Pb}$ optical potential at 149 MeV (7/8 of the incident energy) and the KD02 systematics [49] were used for the $p + ^{208}\text{Pb}$ potential at 21.3 MeV (1/8 of the incident energy). The calculated total reaction and total breakup cross sections were 3888 mb and 633 mb, respectively.

As shown in Fig. 5, the CDCC calculation describes the measured elastic-scattering angular distribution very well. The calculation without taking into account the breakup-channel couplings does not differ from that of the full CDCC

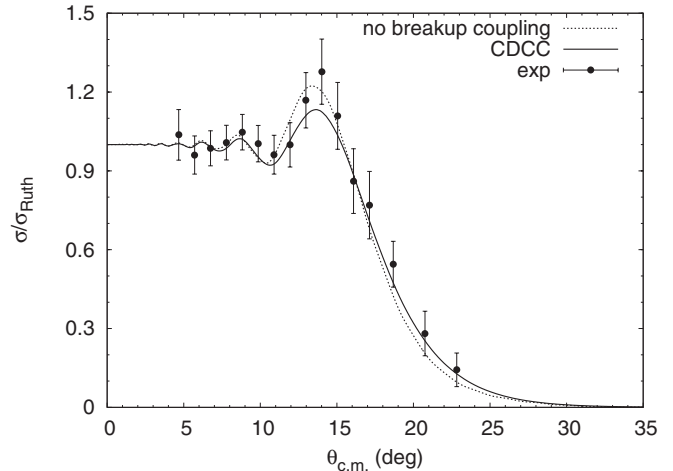


FIG. 5. Elastic scattering of ^8B from ^{208}Pb at 170.3 MeV with and without taking into account couplings to breakup channels calculated within the CDCC formalism, represented by the solid and dotted curves, respectively. Note the linear cross section scale.

calculation as much as that was found for near-barrier $^{11}\text{Be} + ^{64}\text{Zn}$ quasielastic scattering [13,29] or ^6He elastic scattering from heavy targets [8–11], in which a strong reduction of the CNIP, largely due to breakup couplings, was observed.

IV. SUMMARY AND CONCLUSIONS

New data for the $^8\text{B} + ^{\text{nat}}\text{Pb}$ elastic scattering at an incident energy of around three times the Coulomb barrier were presented. Even with a low beam intensity and broad beam profile the experiment was performed successfully using two PPACs, two ΔE - E silicon detector telescopes and Monte Carlo simulations. The experimental data were well reproduced by an optical model calculation with a systematic single-folding type nucleus-nucleus potential. Coupled-channel calculations were performed to show that the inelastic cross sections are small over the entire angular range of the measurement, thus the data may be regarded as pure elastic scattering for all practical purposes.

CDCC calculations suggest that the effect of breakup-channel couplings on the elastic scattering is small for the present proton-rich projectile at an incident energy well above the Coulomb barrier, which is very different from that observed for the elastic scattering of light neutron-rich nuclei such as ^{11}Be , and ^6He on medium-mass (^{11}Be) or heavy (^6He) targets at near-barrier energies, for which a strong suppression of the CNIP due to breakup couplings seems to be a common feature. However, it is consistent with the results of CDCC calculations for near-barrier $^8\text{B} + ^{58}\text{Ni}$ elastic scattering [50], which found that breakup couplings had an essentially negligible influence on the elastic scattering.

While coupling effects in general become less important as the incident energy is increased above the Coulomb barrier, given the extremely low breakup threshold for ^8B one might naively have expected a rather larger influence of breakup coupling on the elastic scattering for these data, particularly as the total breakup cross section is still about 16% of the

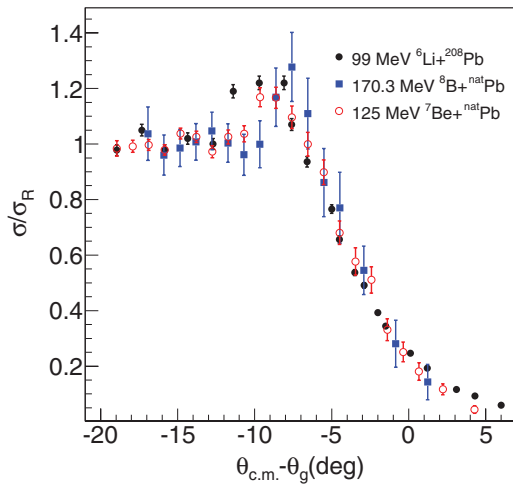


FIG. 6. (Color online) Data for 99 MeV ${}^6\text{Li} + {}^{208}\text{Pb}$ elastic scattering [40], 125 MeV ${}^7\text{Be} + \text{natPb}$ quasielastic scattering [30], and 170.3 MeV ${}^8\text{B} + \text{natPb}$ quasielastic scattering plotted as a function of $\theta_{\text{c.m.}} - \theta_{\text{g}}$. Note the linear cross section scale.

total reaction cross section even at this relatively high energy (see, e.g., Fig. 3 of Ref. [28] for an illustration of how the importance of the contribution of the calculated total breakup cross section to the total reaction cross section steadily reduces as the incident energy is increased). Instead, the main effect is a slight ($\sim 5\%$) reduction of the CNIP. If we plot the data sets for ${}^6\text{Li} + {}^{208}\text{Pb}$ elastic scattering and ${}^7\text{Be}$, and ${}^8\text{B} + \text{natPb}$ quasielastic scattering as a function of the scattering angle minus the grazing angle (defined by the quarter point recipe) in order to remove the small dependence on the nuclear size, we find that within the experimental errors the angular distributions are identical; see Fig. 6.

We therefore confirm the apparent paradox that, for ${}^8\text{B}$, an important set of channels from the point of view of their contribution to the total reaction cross section—the

${}^8\text{B} \rightarrow {}^7\text{Be} + p$ breakup—have a small influence on the elastic scattering. This is spite of the much heavier target than for the previous measurements of Ref. [28]; in the present case Coulomb breakup effects should be at a maximum. However, a test calculation in which Coulomb breakup couplings were omitted (while retaining the diagonal Coulomb potentials) found that while the Coulomb contribution to the total breakup cross section is dominant, as would be expected for such a heavy target, its influence on the elastic scattering is almost negligible. In spite of its very low breakup threshold (0.1375 MeV for ${}^8\text{B} \rightarrow {}^7\text{Be} + p$) we find that the (quasi)elastic-scattering angular distribution for ${}^8\text{B} + \text{natPb}$ at approximately three times the Coulomb barrier energy is essentially identical to those for ${}^6\text{Li}$ (${}^4\text{He} + d$ breakup threshold 1.4643 MeV) and ${}^7\text{Be}$ (${}^4\text{He} + {}^3\text{He}$ breakup threshold 1.5866 MeV) at similar relative energies. The present data make an important contribution to the process of unravelling the enigma that is ${}^8\text{B}$, but further work, both experimental and theoretical, is clearly needed before we fully understand this fascinating nucleus.

ACKNOWLEDGMENTS

We would like to acknowledge the staff of HIRFL for the operation of the cyclotron and friendly collaboration. We are grateful to Dr. H. W. Wang and Dr. W. D. Tian for informative discussions. This work was financially supported by the National Natural Science Foundation of China (Grants No. 11005127, No. 11075190, No. 10905076, No. 11275018, No. 11205209, and No. 11205221), the Directed Program of Innovation Project of Chinese Academy Sciences (Grant No. KJ CX2-YW-N44), and the National Basic Research Program of China (973 program, 2013CB834401). One of the authors (S.M.) acknowledges financial help from UNESCO-TWAS, Trieste, Italy.

-
- [1] B. Jonson, *Phys. Rep.* **389**, 1 (2004).
 [2] N. Keeley *et al.*, *Prog. Part. Nucl. Phys.* **59**, 579 (2007).
 [3] N. Keeley *et al.*, *Prog. Part. Nucl. Phys.* **63**, 396 (2009).
 [4] R. E. Warner *et al.*, *Phys. Rev. C* **51**, 178 (1995).
 [5] G. M. Ter-akopian *et al.*, *Phys. Lett. B* **426**, 251 (1998).
 [6] E. A. Benjamim *et al.*, *Phys. Lett. B* **647**, 30 (2007).
 [7] L. Acosta *et al.*, *Phys. Rev. C* **84**, 044604 (2011).
 [8] O. R. Kakuee *et al.*, *Nucl. Phys. A* **765**, 294 (2006).
 [9] K. Rusek, N. Keeley, K. W. Kemper, and R. Raabe, *Phys. Rev. C* **67**, 041604(R) (2003).
 [10] O. R. Kakuee *et al.*, *Nucl. Phys. A* **728**, 339 (2003).
 [11] A. M. Sánchez-Benítez *et al.*, *Nucl. Phys. A* **803**, 30 (2008).
 [12] R. C. Johnson, J. S. Al-Khalili, and J. A. Tostevin, *Phys. Rev. Lett.* **79**, 2771 (1997).
 [13] A. Di Pietro *et al.*, *Phys. Rev. Lett.* **105**, 022701 (2010).
 [14] I. Tanihata *et al.*, *Phys. Lett. B* **206**, 592 (1988).
 [15] R. E. Warner *et al.*, *Phys. Rev. C* **52**, R1166 (1995).
 [16] M. M. Obuti *et al.*, *Nucl. Phys. A* **609**, 74 (1996).
 [17] F. Negoita *et al.*, *Phys. Rev. C* **54**, 1787 (1996).
 [18] M. Fukuda *et al.*, *Nucl. Phys. A* **656**, 209 (1999).
 [19] W. Schwab *et al.*, *Z. Phys. A* **350**, 283 (1995).
 [20] J. H. Kelley *et al.*, *Phys. Rev. Lett.* **77**, 5020 (1996).
 [21] M. H. Smedberg *et al.*, *Phys. Lett. B* **452**, 1 (1999).
 [22] T. Minamisono *et al.*, *Phys. Rev. Lett.* **69**, 2058 (1992).
 [23] T. Sumikama *et al.*, *Phys. Rev. C* **74**, 024327 (2006).
 [24] E. F. Aguilera *et al.*, *Phys. Rev. Lett.* **107**, 092701 (2011).
 [25] I. Pecina *et al.*, *Phys. Rev. C* **52**, 191 (1995).
 [26] G. Tabacaru *et al.*, *Phys. Rev. C* **73**, 025808 (2006).
 [27] A. Barioni *et al.*, *Phys. Rev. C* **84**, 014603 (2011).
 [28] E. F. Aguilera *et al.*, *Phys. Rev. C* **79**, 021601(R) (2009).
 [29] A. Di Pietro *et al.*, *Phys. Rev. C* **85**, 054607 (2012).
 [30] Y. Y. Yang *et al.*, *Nucl. Instrum. Methods Phys. Res., Sect. A* **701**, 1 (2013).
 [31] Z. Sun *et al.*, *Chin. Phys. Lett.* **15**, 790 (1998).
 [32] Z. Sun *et al.*, *Nucl. Instrum. Methods Phys. Res., Sect. A* **503**, 496 (2003).
 [33] J. W. Xia *et al.*, *Nucl. Instrum. Methods Phys. Res., Sect. A* **488**, 11 (2002).
 [34] W. L. Zhan *et al.*, *Nucl. Phys. A* **805**, 533c (2008).
 [35] Y. P. Xu and D. Y. Pang, *Phys. Rev. C* **87**, 044605 (2013).
 [36] D. Y. Pang, Y. L. Ye, and F. R. Xu, *Phys. Rev. C* **83**, 064619 (2011).

- [37] D. Y. Pang, Y. L. Ye, and F. R. Xu, *J. Phys. G* **39**, 095101 (2012).
- [38] E. Bauge, J. P. Delaroche, and M. Girod, *Phys. Rev. C* **58**, 1118 (1998).
- [39] E. Bauge, J. P. Delaroche, and M. Girod, *Phys. Rev. C* **63**, 024607 (2001).
- [40] D. P. Stanley, F. Petrovich, and P. Schwandt, *Phys. Rev. C* **22**, 1357 (1980).
- [41] G. R. Satchler, *Nucl. Phys. A* **329**, 233 (1979).
- [42] D. T. Khoa, H. S. Than, T. H. Nam, M. Grasso, and N. V. Giai, *Phys. Rev. C* **69**, 044605 (2004).
- [43] H. De Vries, C. W. De Jager, and C. De Vries, *At. Data Nucl. Data Tables* **36**, 503 (1987).
- [44] B. A. Brown, *Phys. Rev. C* **58**, 220 (1998).
- [45] J. Zenihiro *et al.*, *Phys. Rev. C* **82**, 044611 (2010).
- [46] I. J. Thompson, *Comput. Phys. Rep.* **7**, 167 (1988).
- [47] P. R. Christensen, S. Pontoppidan, F. Videbaek, J. Barrette, P. D. Bond, O. Hansen, and C. E. Thorn, *Phys. Rev. C* **29**, 455 (1984).
- [48] P. Navrátil, C. A. Bertulani, and E. Caurieri, *Phys. Lett. B* **634**, 191 (2006).
- [49] A. J. Koning and J. P. Delaroche, *Nucl. Phys. A* **713**, 231 (2003).
- [50] J. Lubian, T. Correa, E. F. Aguilera, L. F. Canto, A. Gomez-Camacho, E. M. Quiroz, and P. R. S. Gomes, *Phys. Rev. C* **79**, 064605 (2009).